 Related Commentary, page 3828

Nitisinone improves eye and skin pigmentation defects in a mouse model of oculocutaneous albinism

Ighovie F. Onojafe,[1] David R. Adams,[2] Dimitre R. Simeonov,[2] Jun Zhang,[3] Chi-Chao Chan,[3] Isa M. Bernardini,[2] Yuri V. Sergeev,[1] Monika B. Dolinska,[1] Ramakrishna P. Alur,[1] Murray H. Brilliant,[4] William A. Gahl,[2] and Brian P. Brooks[1]

[1]Unit on Pediatric, Developmental, and Genetic Eye Disease, National Eye Institute, NIH, Bethesda, Maryland, USA. [2]Section on Human Biochemical Genetics, Medical Genetics Branch, National Human Genome Research Institute, NIH, Bethesda, Maryland, USA. [3]Section of Immunopathology, National Eye Institute, NIH, Bethesda, Maryland, USA. [4]Center for Human Genetics, Marshfield Clinic, Marshfield, Wisconsin, USA.

Mutation of the tyrosinase gene (*TYR*) causes oculocutaneous albinism, type 1 (OCA1), a condition characterized by reduced skin and eye melanin pigmentation and by vision loss. The retinal pigment epithelium influences postnatal visual development. Therefore, increasing ocular pigmentation in patients with OCA1 might enhance visual function. There are 2 forms of OCA1, OCA-1A and OCA-1B. Individuals with the former lack functional tyrosinase and therefore lack melanin, while individuals with the latter produce some melanin. We hypothesized that increasing plasma tyrosine concentrations using nitisinone, an FDA-approved inhibitor of tyrosine degradation, could stabilize tyrosinase and improve pigmentation in individuals with OCA1. Here, we tested this hypothesis in mice homozygous for either the $Tyr^{c\text{-}2J}$ null allele or the $Tyr^{c\text{-}h}$ allele, which model OCA-1A and OCA-1B, respectively. Only nitisinone-treated $Tyr^{c\text{-}h/c\text{-}h}$ mice manifested increased pigmentation in their fur and irides and had more pigmented melanosomes. High levels of tyrosine improved the stability and enzymatic function of the $Tyr^{c\text{-}h}$ protein and also increased overall melanin levels in melanocytes from a human with OCA-1B. These results suggest that the use of nitisinone in OCA-1B patients could improve their pigmentation and potentially ameliorate vision loss.

Introduction

Oculocutaneous albinism (OCA) is an autosomal-recessive condition characterized by reduced pigmentation of the hair, skin, and eyes (1, 2). Common ocular features of OCA include iris transillumination, nystagmus, foveal hypoplasia, and reduced best-corrected visual acuity; children have varying degrees of visual impairment and can be legally blind. The mechanism of reduced visual acuity and overall visual function is multifactorial and involves foveal hypoplasia, nystagmus (with reduced foveation time), refractive errors, photosensitivity, and developmental abnormalities of the visual pathways, including abnormal decussation of ganglion cell axons at the optic chiasm (3–7). Current treatment options for children with albinism are limited to correction of refractive errors, treatment of amblyopia (if present), low vision aids, and, in some cases, extraocular muscle surgery (8). Often, however, significant visual impairment persists.

Traditionally, patients with OCA have been divided into those who show tyrosinase activity on hair bulb testing (tyrosinase positive) and those who do not (tyrosinase negative). In the era of molecular genetics, nonsyndromic OCA has been classified based on the gene that is mutated: the tyrosinase gene (*TYR*) causes OCA1 (9–12), *OCA2* (previously known as the P gene) causes OCA2 (13, 14), tyrosinase-related protein-1 gene (*TYRP1*) causes OCA3 (15), and *SLC45A2* (previously known as *MATP* and *AIM1*) causes OCA4 (16). OCA1, the most common form of OCA in North American white individuals (17, 18), with a prevalence of approximately 1:36,000 (19), can be further divided into a disorder with complete absence of tyrosinase activity (OCA-1A) and a disorder with residual tyrosinase activity (OCA-1B). Tyrosinase catalyzes the initial, rate-limiting steps in pigment (melanin) production in the skin and eye (20, 21); melanin is a complex biomolecule synthesized and is stored in organelles called melanosomes. Melanosomes mature through 4 recognizable stages. Stages I and II are early, premelanosome organelle containing little or no pigment. Stages III (late premelanosome) and IV (mature melanosomes) contain increasing amounts of pigment.

Although the early developmental abnormalities associated with OCA (e.g., abnormal decussation of fibers at the optic chiasm) may be difficult to correct, later aspects of visual development may prove more tractable. In particular, the maturation of the macula and fovea are known to continue peri- and postnatally and are therefore more amenable to intervention (22–24). The mechanistic role that tyrosinase activity and/or pigment formation have in this process is not well understood, but a rough correlation exists between visual function and the amount of fundus pigmentation (3).

We postulate that increasing pigmentation may improve the visual function of individuals with albinism. In adults, benefit may be limited to symptoms associated with glare and photosensitivity, but infants may realize more dramatic effects if retinal development can be partially restored. In vitro and ex vivo experiments in animal models of OCA have suggested that increasing ambient levels of tyrosine (the substrate for tyrosinase) to millimolar levels may stabilize the enzyme, aid in its proper targeting to the melanosome, and increase pigment production (25, 26). Lopez et al. have proposed that the initial product of tyrosinase,

Conflict of interest: Brian P. Brooks, William A. Gahl, and David R. Adams have a patent pending for the use of nitisinone for disorders of hypopigmentation in humans.

Citation for this article: *J Clin Invest.* 2011;121(10):3914–3923. doi:10.1172/JCI59372.

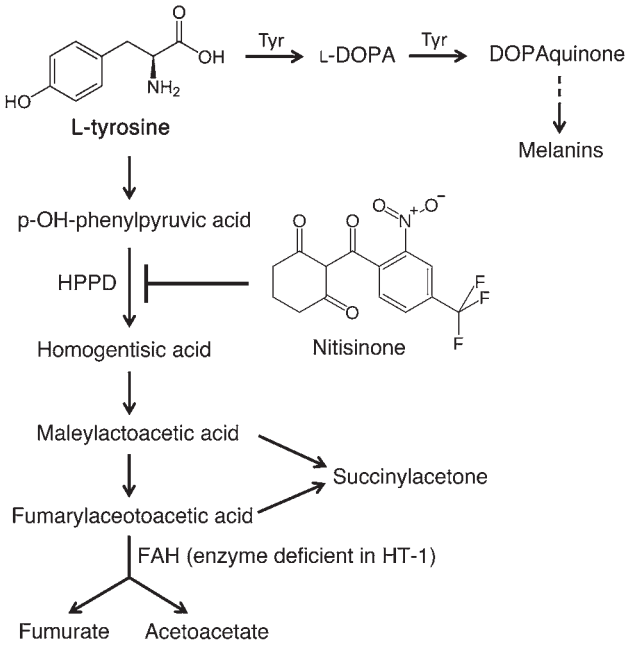

Figure 1
Tyrosine degradation and melanin synthesis. The HPPD inhibitor nitisinone elevates plasma tyrosine concentrations in humans. It is used clinically in the treatment of HT-1 due to deficient FAH activity. Tyr is the first and rate-limiting step in the production of melanin.

L-DOPA, binds to the retinal pigment epithelium (RPE) melanosomal protein GPR143 (previously termed OA1) and stimulates the release of a neurotrophic factor, PEDF (also known as serpin F1), which may affect retinal development (27). Furthermore, basic principles of Michaelis-Menten kinetics support the notion that increasing substrate concentration up to several times the K_m will increase product formation.

An inhibitor of 4-hydroxyphenylpyruvate dioxygenase, nitisinone [Orfadin; 2(-2-nitro-4 trifluoromethylbenzoyl)-1,3 cyclohexanedione] is an FDA-approved drug for the treatment of hereditary tyrosinemia type 1 (HT-1) caused by deficient fumarylacetoacetate hydrolase (FAH) activity (Figure 1 and refs. 28–31). This drug competitively inhibits 4-hydroxyphenylpyruvate dioxygenase, an enzyme upstream of FAH in the tyrosine catabolic pathway. Inhibition of tyrosine catabolism prevents the accumulation of the toxic intermediate maleylacetoacetate and fumarylacetoacetate, which destroy the liver and kidney of HT-1 patients. As a side effect of nitisinone treatment, plasma tyrosine levels are elevated in treated HT-1 patients, but the magnitude of elevation is reduced by coinstitution of a low-protein diet. The pharmacokinetics, pharmacodynamics, and toxicology of nitisinone have been well studied in mice and humans (28–32). Standard doses of 1–2 mg/kg/d in humans and up to 160 mg/kg/d in mice have been well tolerated (33, 34).

In the present study, we demonstrated that administering nitisinone to mice with reduced tyrosinase activity elevated plasma tyrosine levels and increased pigmentation. These findings have important therapeutic implications for enhancing the visual acuity of patients with OCA-1B.

Results

Nitisinone increases coat and iris pigmentation in a mouse model of OCA-1B. We administered nitisinone to 2 isogenic mouse models of OCA. The $Tyr^{c\text{-}2J/c\text{-}2J}$ mouse, a model of OCA-1A, is phenotypically albino due to a mutation in the *Tyr* gene (c.G291T, p.R77L); it was a functional null at the protein level (Figure 2B, Figure 3D, Figure 4B, and refs. 35, 36). The $Tyr^{c\text{-}h/c\text{-}h}$ mouse (also known as the Himalayan mouse), a model of OCA-1B, is homozygous for a *Tyr* allele that has maximum enzymatic activity below normal body temperature (37°C) because the mutant protein (c.A1259G, p.H420R) is heat labile (37, 38). In homozygotes, the first coat was a uniform light tan. At the first molt, the body hair became lighter, and the ears, nose, tail, and scrotum became dark (Figure 2C), as in Siamese cats. Eyes were minimally pigmented and appeared red (Figure 3C, Figure 4C, and ref. 39). WT mice (C57BL6/J) had a black coat color and a dark brown fundus upon dilated eye examination (Figure 2A and Figure 4A). Because their dark brown iris pigmentation blocked light reflected off the back of the eye, no iris transillumination was observed in WT mice upon slit lamp examination (Figure 3, A and B). Iris transillumination is a cardinal finding in patients with OCA.

A nitisinone dose of 4 mg/kg, given every other day by oral gavage, produced approximately 60% of the maximal elevation of plasma tyrosine concentration achievable without discernible side effects (Supplemental Figure 1; supplemental material available online with this article; doi:10.1172/JCI59372DS1). After 1 month of nitisinone treatment, plasma tyrosine levels were elevated 4- to 6-fold compared with placebo-treated controls (Table 1). $Tyr^{c\text{-}h/c\text{-}h}$ mice, but not $Tyr^{c\text{-}2J/c\text{-}2J}$ mice, showed increased pigmentation in areas of new hair growth upon physical examination (n = 10 per group; Figure 2, B–E). Note that, because pigment is preferentially

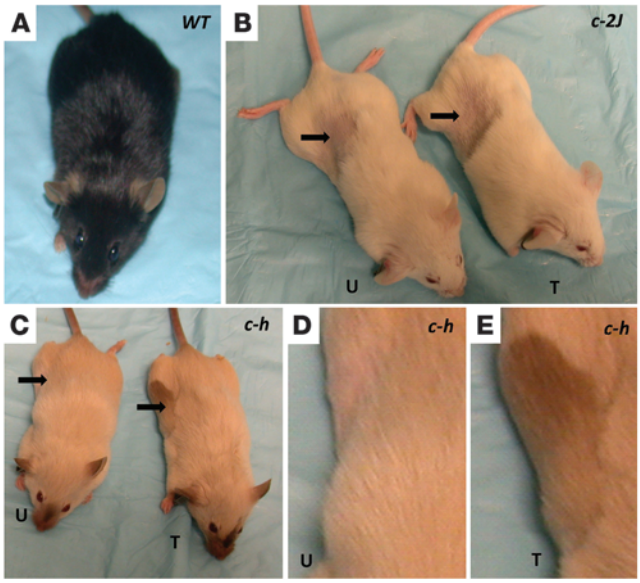

Figure 2
Comparison of nitisinone- and vehicle-treated $Tyr^{c\text{-}2J/c\text{-}2J}$ and $Tyr^{c\text{-}h/c\text{-}h}$ mice. (**A**) WT C57BL6 mouse. (**B** and **C**) Untreated (U) and treated (T) $Tyr^{c\text{-}2J/c\text{-}2J}$ (**B**) and $Tyr^{c\text{-}h/c\text{-}h}$ (**C**) mice at 1 month. A patch of fur was shaved to stimulate new hair growth, which was preferentially pigmented. (**D** and **E**) Close-up images of previously shaved areas of untreated and treated $Tyr^{c\text{-}h/c\text{-}h}$ mice.

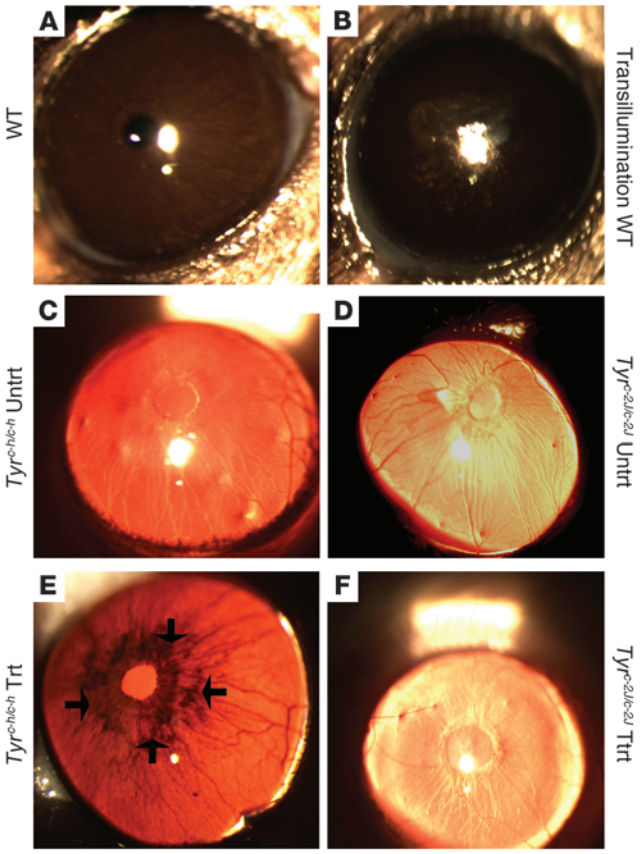

Figure 3
Iris transillumination in treated (Trt) and untreated (Untrt) *Tyr*$^{c\text{-}2J/c\text{-}2J}$ and *Tyr*$^{c\text{-}h/c\text{-}h}$ mice. Dark brown melanin in the iris of WT mice (**A**) prevented the reflection of orange-red light off the mouse retina when a small beam of light was directed coaxially through the pupil at the slit lamp (**B**). The absence of significant pigment in *Tyr*$^{c\text{-}h/c\text{-}h}$ (**C**) and *Tyr*$^{c\text{-}2J/c\text{-}2J}$ mice (**D**) allowed this light to be reflected back to the observer, outlining iris blood vessels. After 1 month of nitisinone treatment, *Tyr*$^{c\text{-}h/c\text{-}h}$ mice (**E**), but not *Tyr*$^{c\text{-}2J/c\text{-}2J}$ mice (**F**), developed demonstrable iris pigment (arrows).

deposited in new hair growth, we stimulated growth in our model by shaving a patch of fur. Similarly, slit lamp examination of the anterior segment showed increased pigmentation in the irides of *Tyr*$^{c\text{-}h/c\text{-}h}$ mice, but not *Tyr*$^{c\text{-}2J/c\text{-}2J}$ mice, as assessed by iris transillumination (Figure 3, E and F). Dilated fundoscopic examination showed no discernible increase in pigmentation in either strain of treated mice (Figure 4, B and C).

Nitisinone increases melanin content in the melanosomes of ocular tissues. In order to quantify the effect of nitisinone on pigmentation in ocular tissues and to assess for subclinical changes in ocular pigmentation, we performed TEM of iris, RPE, and choroid of treated and control mice (n = 4 eyes from 2 mice per group.) When TEM images of iris, choroid, and RPE of nitisinone-treated *Tyr*$^{c\text{-}2J/c\text{-}2J}$ mice were compared with those of untreated mice (n = 10 images per group), little to no increase in the number of pigmented melanosomes (stages III and IV) was observed, consistent with our clinical observations (Figure 5). The small number of pigment granules present in treated mice was irregular and not clearly in melanosomes. In contrast, TEM images of iris, choroid, and RPE of nitisinone-treated *Tyr*$^{c\text{-}h/c\text{-}h}$ mice (n = 10 images per group) showed a significant increase in the number of pigmented melanosomes compared with controls (P < 0.001 in all tissues examined; Figure 6).

Prenatal treatment with nitisinone increases coat and iris pigmentation in Tyr$^{c\text{-}h/c\text{-}h}$ *pups*. In order to assess whether elevation of plasma tyrosine by nitisinone treatment could have an effect early in development, we treated pregnant *Tyr*$^{c\text{-}h/c\text{-}h}$ females with 4 mg/kg nitisinone. Whereas pups of vehicle-treated mothers had coat color similar to that of untreated pups of the same genotype, the pups of nitisinone-treated mothers had considerably darker coats (Figure 7). Ocular examinations performed near the time of weaning showed that irides of pups born to vehicle-treated mothers resembled those of untreated *Tyr*$^{c\text{-}h/c\text{-}h}$ mice. The irides of pups born of nitisinone-treated mothers, however, showed substantial pigmentation upon clinical examination (Figure 7). There was no significant difference between the fundus appearance of pups born to vehicle-treated and drug-treated dams (data not shown). The pups of treated mothers had no obvious congenital malformations, systemic illnesses, or behavioral abnormalities. These data suggest that nitisinone's effectiveness in increasing ocular and cutaneous pigmentation in *Tyr*$^{c\text{-}h/c\text{-}h}$ mice extends into the prenatal/neonatal period.

In silico modeling of mouse tyrosinase mutations agrees with in vivo observations. We hypothesized that nitisinone exerts its pigment-increasing effect in *Tyr*$^{c\text{-}h/c\text{-}h}$ mice by increasing tyrosine concentrations, which in turn stabilizes the tyrosinase protein. In order to explain the differing effects of nitisinone on the 2 OCA models studied, we modeled the predicted effect of the *Tyr*$^{c\text{-}2J/c\text{-}2J}$ (R77L) and *Tyr*$^{c\text{-}h}$ (H420R) tyrosinase mutants in silico (Supplemental Results). Because X-ray crystallography has not been successfully performed on mammalian tyrosinase, the homology-modeling analyses previously reported and presented here rely, in part, on the available crystal structures of prokaryotic (*Streptomyces castaneoglobisporus*) and mushroom tyrosinase, invertebrate hemocyanin, and plant catechol oxidase (Supplemental Figures 2 and 3 and refs. 40–45). The active site structure of mouse tyrosinase predicted by homology modeling (see Methods) is demonstrated in Figure 8A, superimposed with copper-bound prokaryotic tyrosinase as a structural template.

The *Tyr*$^{c\text{-}2J}$ mutation, R77L, occurs in a structural fragment at the amino terminus that is identified by the Simple Modular Architecture Research Tool (SMART; http://smart.embl-heidelberg.de/) as an EGF/laminin-like domain. While the precise function

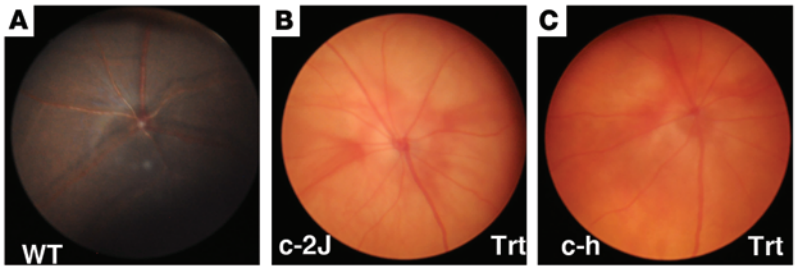

Figure 4
Fundus photos. (**A**) WT. (**B**) Treated *Tyr*$^{c\text{-}2J/c\text{-}2J}$. (**C**) Treated *Tyr*$^{c\text{-}h/c\text{-}h}$. Neither *Tyr*$^{c\text{-}2J/c\text{-}2J}$ nor *Tyr*$^{c\text{-}h/c\text{-}h}$ mice demonstrated any clinical difference in fundus pigmentation after 1 month of nitisinone treatment.

Table 1
Plasma tyrosine after 1 month of nitisinone treatment

	n	Plasma tyrosine	*P* vs. control
$Tyr^{c\text{-}2J/c\text{-}2J}$			
Control	6	109 ± 30 μM	
Nitisinone	4	678 ± 73 μM	1×10^{-7}
$Tyr^{c\text{-}h/c\text{-}h}$			
Control	6	74 ± 25 μM	
Nitisinone	4	305 ± 35 μM	2×10^{-6}

Mice in the treatment group received 4 mg/kg nitisinone every other day.

of this domain is not known, the R77L mutation is predicted to have major structural consequences based on its negative blosum 70 score of –3 and significant Grantham distance of 102. Blosum 70 scores indicate the likelihood of an amino acid substitution across species, with a negative score indicating a lower likelihood of a particular substitution being observed (46). Grantham distance indicates the degree of amino acid difference using a combination of physicochemical features, such as composition, polarity, and molecular volume, that correlate best with protein residue substitution frequencies (47). Structure equilibration using 3ps molecular dynamics suggested that the mutational change had a dramatic effect on tyrosine binding, which is thought to occur at the hydrophobic surface of the catalytic site (Figure 8B, Supplemental Figure 2, and refs. 44, 45). The replacement of a large, positively charged R77 with L is predicted to cause a destabilizing structural change in a loop including amino acid residues 188–199 by disrupting 3 native hydrogen bonds between R185 and D199, as well as altering the positions of 2 surface residues, W195 and I194, in the hydrophobic tyrosine-binding pocket. We therefore anticipate that elevating ambient tyrosine concentrations would have little to no effect on baseline enzyme function, in agreement with our in vivo results.

In contrast, the $Tyr^{c\text{-}h}$ mutation, H420R, demonstrated a blosum 70 score of 0 and a smaller Grantham distance of 29, both of which suggest a less severe structural change. Rather than directly affecting the structure of the hydrophobic tyrosine binding pocket, our model predicts a greater effect on the coordination of copper near the active site (Figure 8C). The 3ps molecular dynamics equilibration in water predicted a steric shift in the 4-helix bundle at the core of tyrosinase (positions 208–218 and 178–182), altering the position of W210, increasing the gap between helices at positions 208–218 and 178–182, and shifting residues H211 and H180, which coordinate copper at the active site. The introduction of a positive charge disrupts several hydrogen bonds, including the bonds maintaining the orientation of R185. Thus, the H420R mutation is likely to disrupt coordination of a copper in the mouse tyrosinase structure. These results were consistent with our in vivo data, and we predict that elevated tyrosine concentrations — binding at the relatively unaffected hydrophobic cavity — might stabilize the enzyme enough to allow for less efficient copper coordination and residual enzymatic activity.

Elevated tyrosine stabilizes H420R, but not R77L, tyrosinase. Since our in silico analysis suggested that H420R, but not R77L, tyrosinase can effectively bind tyrosine, we hypothesized that elevated ambient tyrosine might stabilize the $Tyr^{c\text{-}h}$ protein. In order to test this hypothesis, we expressed either WT, R77L, or H420R mutant tyrosinase proteins in CHO cells and measured tyrosinase protein stability using cycloheximide to inhibit new protein synthesis. Similar levels of WT and mutant protein expression were observed on Western blots of cell protein lysates at baseline (Figure 8D, inset). As predicted, 1 mM tyrosine improved the stability of the H420R mutant protein (Figure 8F) at later time points (9 and 24 hours) relative to the marker protein GAPDH. Although there was a trend toward stabilization of the R77L mutant with 1 mM tyrosine, this was not statistically significant (Figure 8E). These results agree with the in vivo observations that pharmacological elevation of plasma tyrosine increased pigmentation in $Tyr^{c\text{-}h/c\text{-}h}$ but not $Tyr^{c\text{-}2J/c\text{-}2J}$ mice.

Elevated tyrosine results in increased enzymatic activity and pigment production in melanocytes expressing OCA-1B Tyr alleles in vitro. We also

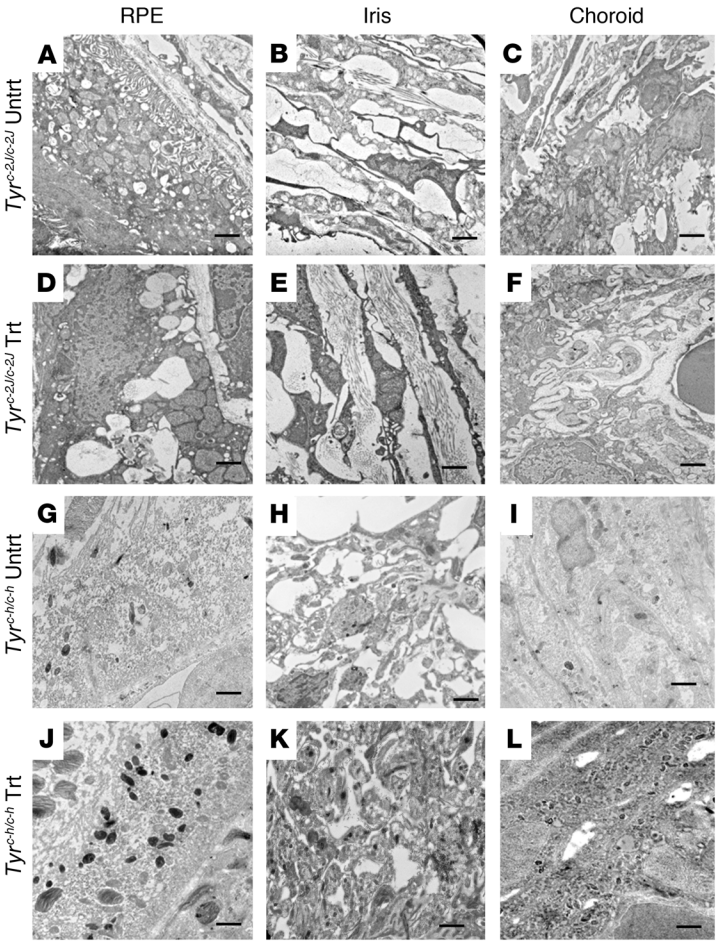

Figure 5
TEM images of RPE, iris, and choroid of treated $Tyr^{c\text{-}2J/c\text{-}2J}$ and $Tyr^{c\text{-}h/c\text{-}h}$ mice. $Tyr^{c\text{-}2J/c\text{-}2J}$ mice showed no discernible pigment in melanosomes, either in the absence of treatment (**A**–**C**) or after 1 month of nitisinone treatment (**D**–**F**). In contrast, $Tyr^{c\text{-}h/c\text{-}h}$ mice showed an appreciable increase in the number of pigmented melanosomes after 1 month of nitisinone treatment (**J**–**L**) compared with untreated mice (**G**–**I**). Scale bars: 500 nm. Original magnification, ×12,000.

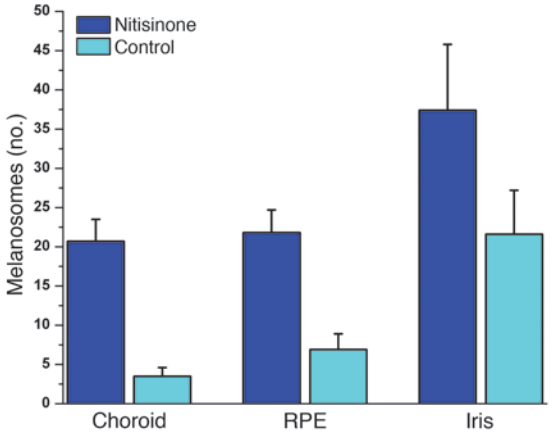

Figure 6
Number of pigmented melanosomes in 10 equally magnified, representative fields of ocular tissues of vehicle- and nitisinone-treated $Tyr^{c\text{-}h/c\text{-}h}$ mice. $P < 0.001$, nitisinone vs. control, in all 3 tissues.

investigated the enzymatic activity of R77L and H420R mutant proteins in vitro compared with WT protein in albino mouse melanocytes (Melan-c cells) (48). Mirroring our in vivo results, 1 mM tyrosine (a saturating concentration) increased enzyme activity over baseline in Melan-c cells expressing the H420R mutant tyrosinase ($P = 0.03$), but not the R77L mutant tyrosinase, despite comparable levels of protein expression (Figure 9, A and B).

In addition, we also investigated the response of human melanocytes cultured from the skin of OCA-1A and OCA-1B patients. Similar to our results with transfected mouse Melan-c cells and our in vivo results, cultured melanocytes from an OCA-1B patient — but not those from an OCA-1A patient — developed a visible increase in pigmentation in response to 1 mM tyrosine ($P = 0.006$; Figure 9, C and F). This effect was not observed in cultured melanocytes treated with 50 nM nitisinone (in which a slight decrease in pigment production was observed; $P = 0.002$; Figure 9D), and the effect of 1 mM tyrosine was not potentiated by the addition of nitisinone (Figure 9E). These in vitro results suggest that elevation of circulating tyrosine may be able to increase pigmentation in humans with residual tyrosinase activity and imply that the effect observed in $Tyr^{c\text{-}h/c\text{-}h}$ mice may be generalizable to other hypomorphic alleles of *TYR*/*Tyr*. These data also suggest that nitisinone is acting via elevating plasma tyrosine and not via an indirect mechanism.

Discussion

Here, we demonstrated that nitisinone elevated tyrosine in both the $Tyr^{c\text{-}2J/c\text{-}2J}$ and the $Tyr^{c\text{-}h/c\text{-}h}$ mouse models of albinism (modeling OCA-1A and OCA-1B, respectively), but only $Tyr^{c\text{-}h/c\text{-}h}$ mice exhibited increased ocular and cutaneous pigmentation after 1 month of treatment. This effect was observed with both prenatal and postnatal treatment. We also presented in silico and in vitro evidence that elevation of plasma tyrosine stabilizes the $Tyr^{c\text{-}h}$ mutant protein, resulting in residual enzyme activity and pigment production. Finally, we showed that elevation of ambient tyrosine increased total enzyme activity and/or pigmentation of both Melan-c cells expressing the H420R mouse mutant tyrosinase and melanocytes cultured from an OCA-1B patient, but not an OCA-1A patient, which argues that hypertyrosinemia may have clinically beneficial effects in humans with residual tyrosinase activity. The proportion of OCA1 patients with residual tyrosinase activity who might benefit from nitisinone treatment is unknown; however, many of the reported variants in OCA1 have been associated with an OCA-1B phenotype (49). Our observation that elevated tyrosine improved pigmentation in OCA-1B human melanocytes with mutation(s) distinct from the $Tyr^{c\text{-}h/c\text{-}h}$ mouse implies that nitisinone treatment may be useful in a spectrum of albinism patients with residual tyrosinase activity.

Individuals with OCA-1B have partially intact processing, targeting, and enzymatic activity of tyrosinase. This allows for 2 therapeutic mechanisms of action of nitisinone with respect to its elevation of plasma tyrosine concentrations. The first is to improve tyrosinase targeting, folding, and stability, and therefore its total enzymatic activity. The second is to permit tyrosinase to act on its substrate, tyrosine, at a concentration above the K_m. The published K_m values for tyrosinase with respect to tyrosine are in the range of 100–500 μM (50–53). While the concentrations of tyrosine within the melanosome itself are unknown, nitisinone at 4 mg/kg elevated plasma tyrosine concentrations to nearly 700 μM in mice; treatment of humans with nitisinone at 2 mg per day resulted in mean plasma tyrosine levels of approximately 800 μM (normal range, ≈10–80 μM) (34). Such levels allow tyrosinase to act closer to its maximum velocity.

Another important finding was that the enhanced pigmentation assessed in ocular tissues of $Tyr^{c\text{-}h/c\text{-}h}$ mice reflected increased melanin content within intracellular melanosomes. This proper compartmentalization of melanin is likely important in avoiding the possible toxic effects of ectopic pigment formation. Melanin production involves the polymerization of DOPAquinone intermediates that can produce toxic oxygen free radicals and cellular damage (54); it has been proposed that melanosomes have evolved as a means to sequester this otherwise toxic molecule. In fact, substantial cell death was observed when WT tyrosinase was expressed

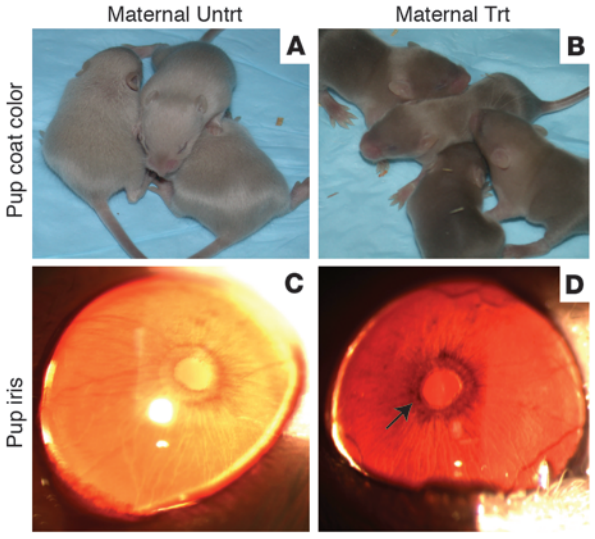

Figure 7
Coat color and iris pigmentation in $Tyr^{c\text{-}h/c\text{-}h}$ pups after prenatal treatment with nitisinone. Pups of treated mothers displayed a darker initial coat color and, at weaning, showed iris pigmentation similar to that observed in treated adult mice.

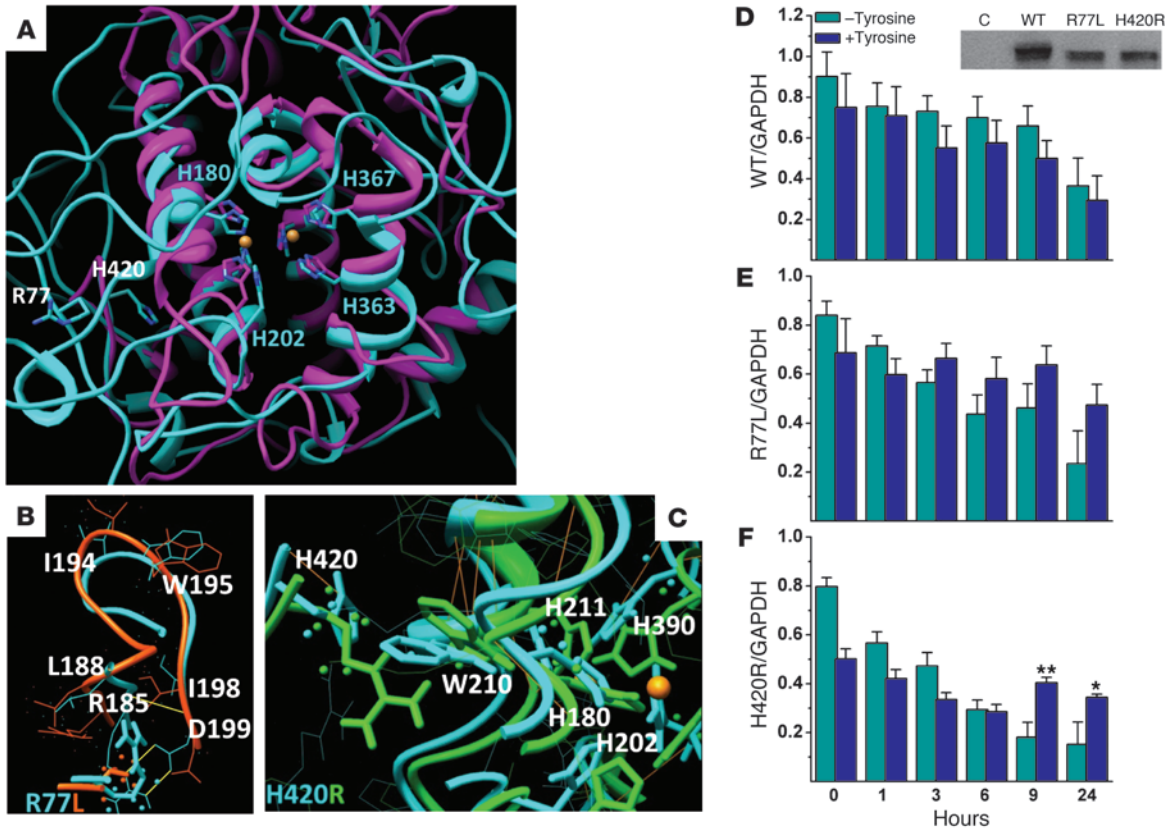

Figure 8

Structure and protein stability of WT and mutant mouse tyrosinase. (**A**) WT mouse tyrosinase (cyan throughout) superimposed with *S. castaneoglobisporus* tyrosinas (magenta), including the dicopper binding active site (orange spheres). Positions of 4 of the 6 critical Hs in the active site as well as the position of the 2 mouse mutations are labeled. (**B** and **C**) Predicted structural effect of (**B**) R77L mutation (orange) and (**C**) H420R mutation (green) on mouse tyrosinase. In **B**, disruption of 3 native hydrogen bonds between R185 and D199 is shown in yellow. See Results for details. (**D**–**F**) Although steady-state levels of WT, R77L, and H420R tyrosinase cell protein lysates were similar (**D**, inset), H420R — but not R77L — was stabilized relative to GAPDH at later time points (9 and 24 hours) by 1 mM tyrosine. C, negative control. $^{*}P < 0.05$, $^{**}P < 0.0001$ vs. no tyrosine.

in CHO cells (lacking melanosomes) in the presence of elevated tyrosine (data not shown); the inability to sequester the toxic intermediates of melanin production may prove fatal to these cells. Hence, compartmentalization of melanin in $Tyr^{c\text{-}h/c\text{-}h}$ mouse melanosomes is a reassuring finding.

In contrast to $Tyr^{c\text{-}h/c\text{-}h}$ mice, $Tyr^{c\text{-}2J/c\text{-}2J}$ mice showed minimally increased production of melanin upon nitisinone treatment, with no evidence that the increased pigment was within melanosomes. Although no overt toxicity was observed in $Tyr^{c\text{-}2J/c\text{-}2J}$ mice under the conditions studied, we would be cautious in considering pharmacologic tyrosine elevation as a treatment strategy for patients with clinical OCA-1A. We chose our mouse model of OCA-1A to be homozygous for a missense mutation in tyrosinase, with the hope that increased tyrosine could serve to stabilize a tyrosinase molecule that — although functionally null — could have some residual enzyme activity restored. Other OCA-1A–causing mutations may prove more amenable to therapy with nitisinone-induced hypertyrosinemia. Both our in vitro culturing of melanocytes from humans with OCA and our ability to express functional mutant *Tyr* in Melan-c cells provide methods for assessing whether any given mutant protein might respond to elevated tyrosine.

A significant unanswered question is whether improving pigmentation in patients with albinism would improve visual function. While developmental decisions determining the decussation of retinal ganglion cell axons at the optic chiasm are determined during the first trimester of pregnancy (55, 56), foveal maturation in the retina continues postnatally, offering a potential therapeutic window for treatments (57). Moreover, melanin likely captures visible light inside the eye, helping avoid backscattering off the outer ocular tissues, such as the sclera, that would degrade the visual signal. It is therefore biologically plausible that increasing pigmentation, even in adulthood, may help with symptoms such as glare sensitivity and contrast perception. Mice are largely nocturnal animals that rely more on senses such as smell and hearing for their interaction with the environment. They lack a fovea, and the grating visual acuity of an adult pigmented WT mouse is approximately 20/1200 (58), well below that of nearly all patients with albinism (3). Therefore, we would not anticipate (nor did we observe) the small amounts of pigment deposited in the eyes of nitisinone-treated $Tyr^{c\text{-}h/c\text{-}h}$ mice to have a robust effect on overt visual function (our unpublished observations). Whether the increased pigmentation attendant to nitisinone treatment

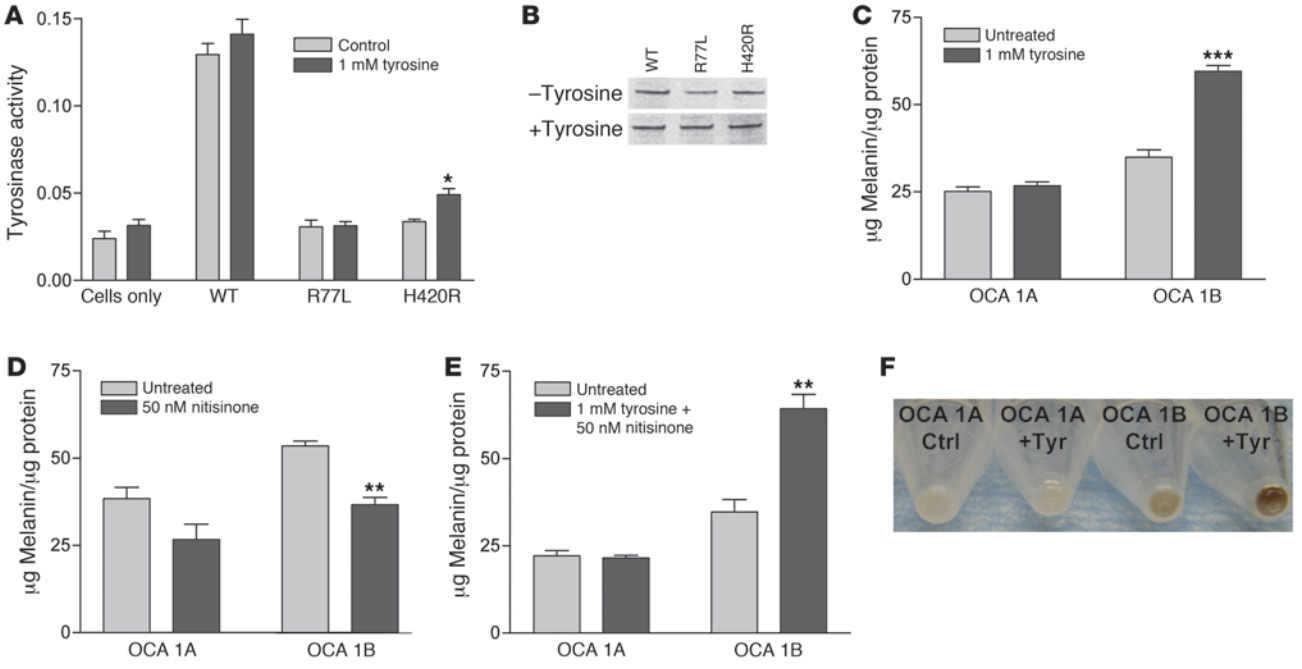

Figure 9

Increased ambient tyrosine promotes tyrosinase enzymatic activity and pigment production in OCA-1B allele-expressing cells. (**A** and **B**) Although Melan-c cells transfected with WT, R77L, or H420R tyrosinase expressed comparable levels of protein, only H420R responded to 1 mM tyrosine by increasing enzyme activity. (**C**–**F**) Melanin production and pigmentation in cultured human melanocytes from an OCA-1B patient and an OCA-1A patient. (**C**) OCA-1B melanocytes — but not OCA-1A melanocytes — showed increased pigment upon incubation with 1 mM tyrosine. Nitisinone itself (50 nM) did not produce this effect in vitro (**D**), nor did it potentiate the response of 1 mM tyrosine (**E**), which suggests that the increase in pigmentation is tyrosine mediated and not an indirect effect of the drug. (**F**) The effect on pigmentation was clearly visible in pellets of cells treated with 1 mM tyrosine. $^{*}P < 0.05$, $^{**}P < 0.01$, $^{***}P = 0.006$ vs. control.

will show demonstrable changes with more subtle quantitative measures, such as electroretinography or — when given prenatally — correction of ganglion cell axon decussation (59), is the subject of ongoing investigations.

Nitisinone is approved by the FDA for use in the treatment of HT-1, along with a special, protein-restricted diet (28). Recent experience with this compound in patients with a related disorder of tyrosine degradation, alkaptonuria, suggests that it can be safely administered to adults receiving a normal diet without significant systemic complications (34). Nitisinone may therefore provide a clinically viable means of increasing pigmentation, and potentially visual function, in patients with OCA-1B. We are currently organizing a pilot clinical study in adults with OCA-1B to test this hypothesis.

Methods

Animal husbandry and clinical examination. WT mice (stock no. 000664; C57BL/6J), *Tyr*$^{c\text{-}2J/c\text{-}2J}$ mice (stock no. 000058, MGI ID 1855985; C57BL/6J background), and *Tyr*$^{c\text{-}h/c\text{-}h}$ mice (stock no. 000104, MGI ID 1855979; C57BL/6 background) were obtained from The Jackson Laboratory. Mice were housed according to our institutional Animal Review Board standards with a 14-hour light/10-hour dark cycle. Clinical examination and imaging of the anterior segment of mice were performed on gently restrained awake mice using a Haag-Streit BQ slit lamp and Imaging Module IM900 software. Clinical examination of the posterior segment was performed on gently restrained awake mice after dilation with 1 drop of 1% tropicamide (Alcon Laboratories Inc.) using an indirect ophthalmoscope (Keeler) with a 90D condensing lens (Volk). Fundus images were obtained on mice sedated with intraperitoneally injected 100 mg/ml ketamine and 200 mg/ml xylazine diluted in normal saline. Images were obtained using a Nikon D.90 digital SLR camera with a Nikon 85 mm f/2.8D micro AF-S ED lens mounted to a custom-made aluminum stand, using a 5-cm-long Hopkins rigid otoscope coupled to a Xenon Nova light source (175 watt) and fiber optic cable (Karl Storz). Mice were euthanized with carbon dioxide according to institutional guidelines.

Drug dosing and monitoring. 10 C57BL/6J *Tyr*$^{c\text{-}2J/c\text{-}2J}$ and 10 C57BL/6 *Tyr*$^{c\text{-}h/c\text{-}h}$ mice aged 3–4 months were designated for treatment with nitisinone (NTBC; Swedish Orphan International); an equal number of age-matched controls of each genotype was designated to receive vehicle treatment. Nitisinone was dissolved in 2 M NaOH and brought to neutral pH before it was administered. Coat color, iris transillumination, and fundus appearance were photodocumented prior to treatment. Because pigment deposition in hair is stimulated with new hair growth, a section of each mouse's coat was shaved prior to the beginning of the experiment. Drug or vehicle was given every other day via oral gavage at a dose of 4 mg/kg in a volume of 0.2–0.3 ml. This dose of nitisinone was chosen to give plasma tyrosine concentrations in the range of 0.3–0.7 mM, or approximately 2 to 4 times the doses typically used in humans with tyrosinemia type 1 (60), and within the limits of the tolerated dose in mice (28). Coat color, iris transillumination, and fundus appearance were photodocumented at the end of 1 month of treatment or vehicle dosing. For prenatal treatment experiments, pregnancy was determined by a maternal weight gain of at least 2 g over 7–9 days after observing a vaginal mucus plug. Treatment with 4 mg/kg nitisinone was initiated daily at day 9 or 10 of pregnancy by

oral gavage and given until birth of the litter. At that point, oral treatment of the mother every other day was initiated until time of weaning.

Plasma tyrosine was assayed from retroorbital blood from mice at 1 week and 4 weeks into treatment. Because the amount of blood that could be obtained from nonterminal bleeds was small, plasma from 2–3 mice was pooled to make a single measurement. Plasma samples were frozen immediately after collection on dry ice. Samples ready for assay were gently thawed, diluted with an equal volume of loading buffer (0.2 M lithium citrate, pH 2.2), and filtered using Vivaspin 500 (3,000 Da molecular weight cutoff; Sartorius Stedman Biotech) spun in a fixed-angle centrifuge at 14,000 *g* for 60 minutes at 16°C–20°C. The supernatant was collected, and tyrosine was quantified on a Biochrom 30 using the manufacturer's specifications.

TEM. Eyes were dissected from drug- and vehicle-treated mice and divided into anterior and posterior segments (n = 4 eyes total from 2 separate mice per group). The iris and posterior part (choroid, RPE, and retina) of the eyes were removed and fixed in 2% glutaraldehyde and 2% paraformaldehyde in 0.1 M sodium phosphate buffer (PB), pH 7.4, for 12 hours at room temperature. After a wash with rinsing buffer (RB; 4% sucrose and 0.15 mM $CaCl_2$ in PB), pH 7.4 at 4°C, tissues were postfixed in 1% OsO_4 in 0.1 M PB, pH 7.4, for 1 hour. After rinsing and dehydration, tissues were embedded in Durcupan resin for 72 hours at 60°C. 1-μm semisections were used for tissue orientation. Then 70- to 90-nm ultrasections were collected in 200 mesh grids and counterstained with 5% uranyl acetate and 0.3% lead citrate. Sections were viewed on a JEOL 1010EM at 60 KV, and digital images were acquired at ×12,000 magnification by AMT software (Advanced Microscopy Techniques Corp.). For each tissue, the number of pigmented (stage III or IV) melanosomes in TEM images of the same magnification were counted by a masked observer in the treated and untreated mice (n = 10 images per group).

Structural modeling. The atomic structure of mouse tyrosinase has been modeled using the crystal coordinates of 2 bicopper-binding tyrosinase proteins from the RCSB protein data bank (PDB; http://www.pdb.org/pdb) as structural templates: (a) *S. castaneoglobisporus* tyrosinase complexed with a caddie protein (PDB ID 2ahl); and (b) the *Ipomea batatas* sweet potato catechol (O-diphenol) oxidase containing dicopper center (PDB ID 1bt3) (61). Briefly, the structural alignment of these proteins was performed using the MatchMaker module incorporated in the UCSF Chimera, build 1.4.1 (62). Primary sequences were aligned using the method of Needleman and Wunsch (63) integrated in the program Look, version 3.5.2, for tertiary structure prediction (64, 65). The location of the major functional components of mouse tyrosinase was predicted by SMART (66, 67). Finally, the monomeric mouse tyrosinase structure was built by the automatic segment matching method in the program Look (68), followed by 500 cycles of energy minimization. The conformation of the missense variants R77L and H420R was generated by the same program implicating a self-consistent ensemble optimization (500 cycles) (65). See Supplemental Methods for further details of molecular modeling (69).

In vitro expression and enzyme activity. The mouse *Tyr* expression construct (provided by C. Olivares, University of Murcia, Murcia, Spain) was prepared in the pcDNA3.1 expression vector (Invitrogen) using EcoRI/XbaI restriction sites and based on the mouse Tyr clone, obtained as described previously (70). Constructs of tyrosinase gene mutant variants with changes corresponding to missense mutations R77L and H420R in the mouse tyrosinase protein sequence were created using standard methodologies (Mutagenex Inc.). All mutational changes were verified by cDNA sequencing. Protein lysates for the WT mouse tyrosinase R77L and H420R missense variants were electrophoretically separated under reducing conditions, blotted, and probed with αPEP7 antiserum (gift of V. Hearing, National Cancer Institute, NIH, Bethesda, Maryland, USA), directed against the C-terminal cytosolic extension of Tyr.

CHO cells (gift of J.T. Wroblewski, Georgetown University Medical Center, Washington DC, USA) were grown at 37°C in DMEM media in the presence of 10% fetal bovine serum, 1% penicillin, and 4.5 g proline per 0.5 l media. CHO cells were transfected with either mouse tyrosinase or mutant variants using the pcDNA3.1 expression vector and Lipofectamine LTX reagent according to the manufacturer's instructions (Invitrogen). In the cyclohexamide experiments, cells were treated with cyclohexamide (2 μg/ml) or pretreated with tyrosine (1 mM) for 24 hours before addition of cyclohexamide in the time-course assay (0, 1, 3, 6, 9, and 24 hours). Following the treatment period, cells were harvested with lysis buffer (10 mM sodium phosphate, pH 7.0, 1% Igepal CA-630, and protease inhibitor), and microfuged for 30 minutes at 13,200 *g*, 4°C, to obtain a protein lysate. The total protein content in protein lysates was determined spectrophotometrically at a 280/260 ratio. Protein expression was analyzed by Western blotting, and GAPDH was used as an internal loading control. For the analysis, Western blots were scanned, intensities of protein bands were determined, and the ratio of WT or mutant variant band intensity to that of GAPDH was calculated. Care was taken in choosing nonsaturated images for analysis. Statistical significance was evaluated using an independent, 2-tailed Student's t test.

Melan-c cells (melanocytes derived from mice homozygous for the albino mutation; ref. 48) were cultured in RPMI 1640, pH 6.9, supplemented with 5% FBS, streptomycin-penicillin (100 μg/ml each), 200 nM tetradeconyl phorbol acetate (TPA), and 100 μM β-mercaptoethanol at 37°C in 10% CO_2. Cells were transfected using Fugene HD reagent according to the manufacturer's instructions (Roche) in the presence or absence of 1 mM tyrosine. After 24 hours, cells were washed twice with saline phosphate buffer, harvested in 10 mM sodium phosphate (pH 6.8) containing 1% Igepal CA-630 and protease inhibitor (Roche), and microcentrifuged for 30 minutes at 13,200 *g*, 4°C, to obtain a protein lysate.

Diphenol oxidase activity of tyrosinase was determined spectrophotometrically according to Slominski (71), with minor modifications. Briefly, the reaction mixtures contained 7 mM L-DOPA in 0.1 M sodium phosphate buffer (pH 6.8), and protein lysate (20 mg/ml) was incubated at 37°C and monitored by measuring the absorbance at 475 nm. All experiments were conducted in triplicates.

Human melanocyte culture and melanin assay. Human melanocytes were established from skin punch biopsies. Skin specimens were washed with PBS, then treated with 0.25% trypsin-EDTA (Gibco 25200; Invitrogen) for 2 hours, followed by vigorous vortexing to separate the epidermis. The epidermis was sectioned and attached to scored patches on the bottom of a 6-well polystyrene culture dish before being covered with melanocyte media. 1,000 ml melanocyte media was made from 950 ml Ham's F10 (Gibco 1550; Invitrogen), 25 ml FBS, 5 μg bFGF (Sigma-Aldrich F0291), 10 μg endothelin (Sigma-Aldrich E7764), 7.5 mg IBMX (Sigma-Aldrich 17018), 30 μg cholera toxin (Sigma-Aldrich C8052), 3.3 μg TPA (Sigma-Aldrich P8139), 10 ml penicillin-streptomycin-glutamine, 1 ml fungizone, and 0.22 μm filtered.

Melanocytes were plated on 6-well dishes and grown to confluency. Melanin assays were run in triplicate by supplementing 3 wells per plate with 1 mM tyrosine (Sigma-Aldrich T8566), using the remaining 3 wells as untreated controls. Treatment time was 1 week. Melanocytes from each well were harvested separately by trypsinization and washed twice with 1× PBS. Pellets were resuspended in 400 μl of 1× PBS and sonicated briefly. The lysate was then split to an equal volume of 2N NaOH (300 μl) and incubated at 80°C for 1 hour to solubilize melanin. The OD_{475} was measured and converted to melanin content via a standard curve using synthetic melanin (Sigma-Aldrich M0418). This was normalized to protein content using a bicinchoninic assay kit (BioRad).

Study participants. Research subjects with OCA were ascertained via an IRB-approved clinical research protocol at the National Human Genome Insti-

tute, NIH. OCA-1A and OCA-1B were defined on clinical grounds based on hair, eye, and skin coloration at the time of first clinical exam. In addition to decreased pigmentation in the hair and skin, both patients had ophthalmic abnormalities consistent with albinism, including iris transillumination, nystagmus, decreased visual acuity, and an albinotic fundus with no clear foveal reflex. Molecular confirmation included sequencing of the genes for OCA1 and OCA2 (*TYR* and *OCA2*, respectively). The OCA-1A subject had 2 known disease-causing mutations in *TYR* (c.230A>G, p.R77Q; c.242C>T, p.P81L) and no likely disease-causing variants in *OCA2*. The OCA-1B subject had 1 known disease-causing variant (c.229T>A, p.R77W) in *TYR* and no likely disease-causing mutation in *OCA2*. Up to 63% of OCA-2B patients have no second identifiable *TYR* mutation (66, 72).

Statistics. Unless otherwise indicated, results are mean ± sample SD. *P* values were determined using 2-tailed Student's *t* test. A *P* value less than 0.05 was considered significant.

Study approval. Animal studies conformed to the principles for laboratory animal research outlined by the Animal Welfare Act (NIH/DHHS) and the ARVO Statement for the Use of Animals in Ophthalmic and Vision Research and were approved by the Institutional Animal Care and Use Committee of the National Eye Institute. Human research was in compliance with the Declaration of Helsinki. The human protocol was approved by the IRB of the National Human Genome Research Institute, NIH, and patients or their representatives provided informed consent.

Acknowledgments

The authors thank V. Hearing for the gift of αPEP7 antiserum and review of the manuscript, J.T. Wroblewski for the gift of CHO cells, and C. Olivares for the gift of the mouse tyrosinase expression construct. We thank the intramural programs of the National Eye Institute and the National Human Genome Research Institute, NIH, for funding this research. B.P. Brooks's lab was partially funded by a 1-year seed grant from the Blind Children's Center.

Received for publication June 6, 2011, and accepted in revised form August 3, 2011.

Address correspondence to: Brian P. Brooks, Building 10, Room 10N226, MSC 1860, 10 Center Drive, Bethesda, Maryland 20892, USA. Phone: 301.451.2238; Fax: 301.402.1214; E-mail: brooksb@mail.nih.gov.

1. King RA, Hearing VJ, Creel DJ, Oetting WS. *Albinism*. New York, New York, USA: McGraw-Hill; 2001.
2. King RA, Oetting WS. Oculocutaneous albinism. In: Nordlund JJ, Boissy RE, Hearing VJ, King RA, Oetting WS, Ortonne JP, eds. *The Pigmentary System: Physiology and Pathophysiology*. Malden, Massachusetts, USA: Blackwell Publishing; 2006:694.
3. Summers CG. Vision in albinism. *Trans Am Ophthalmol Soc*. 1996;94:1095–1155.
4. Anderson J, Lavoie J, Merrill K, King RA, Summers CG. Efficacy of spectacles in persons with albinism. *J AAPOS*. 2004;8(6):515–520.
5. Taylor WO. Edridge-Green Lecture, 1978. Visual disabilities of oculocutaneous albinism and their alleviation. *Trans Ophthalmol Soc U K*. 1978;98(4):423–445.
6. Creel DJ, Summers CG, King RA. Visual anomalies associated with albinism. *Ophthalmic Paediatr Genet*. 1990;11(3):193–200.
7. Abadi RV, Pascal E. Visual resolution limits in human albinism. *Vision Res*. 1991;31(7–8):1445–1447.
8. Hertle RW, Anninger W, Yang D, Shatnawi R, Hill VM. Effects of extraocular muscle surgery on 15 patients with oculo-cutaneous albinism (OCA) and infantile nystagmus syndrome (INS). *Am J Ophthalmol*. 2004;138(6):978–987.
9. Giebel LB, Tripathi RK, King RA, Spritz RA. A tyrosinase gene missense mutation in temperature-sensitive type I oculocutaneous albinism. A human homologue to the Siamese cat and the Himalayan mouse. *J Clin Invest*. 1991;87(3):1119–1122.
10. Giebel LB, et al. Tyrosinase gene mutations associated with type IB ("yellow") oculocutaneous albinism. *Am J Hum Genet*. 1991;48(6):1159–1167.
11. Tripathi RK, Strunk KM, Giebel LB, Weleber RG, Spritz RA. Tyrosinase gene mutations in type I (tyrosinase-deficient) oculocutaneous albinism define two clusters of missense substitutions. *Am J Med Genet*. 1992;43(5):865–871.
12. Spritz RA. Molecular genetics of oculocutaneous albinism. *Semin Dermatol*. 1993;12(3):167–172.
13. Ramsay M, et al. The tyrosinase-positive oculocutaneous albinism locus maps to chromosome 15q11.2-q12. *Am J Hum Genet*. 1992;51(4):879–884.
14. Durham-Pierre D, et al. African origin of an intragenic deletion of the human P gene in tyrosinase positive oculocutaneous albinism. *Nat Genet*. 1994; 7(2):176–179.
15. Boissy RE, et al. Mutation in and lack of expression of tyrosinase-related protein-1 (TRP-1) in melanocytes from an individual with brown oculocutaneous albinism: a new subtype of albinism classified as "OCA3". *Am J Hum Genet*. 1996;58(6):1145–1156.
16. Newton JM, et al. Mutations in the human orthologue of the mouse underwhite gene (uw) underlie a new form of oculocutaneous albinism, OCA4. *Am J Hum Genet*. 2001;69(5):981–988.
17. Hutton SM, Spritz RA. Comprehensive analysis of oculocutaneous albinism among non-Hispanic caucasians shows that OCA1 is the most prevalent OCA type. *J Invest Dermatol*. 2008;128(10):2442–2450.
18. Hutton SM, Spritz RA. A comprehensive genetic study of autosomal recessive ocular albinism in Caucasian patients. *Invest Ophthalmol Vis Sci*. 2008; 49(3):868–872.
19. Gronskov K, Ek J, Brondum-Nielsen K. Oculocutaneous albinism. *Orphanet J Rare Dis*. 2007;2:43.
20. Riley PA. Mechanistic aspects of the control of tyrosinase activity. *Pigment Cell Res*. 1993;6(4 pt 1):182–185.
21. Cooksey CJ, et al. Evidence of the indirect formation of the catecholic intermediate substrate responsible for the autoactivation kinetics of tyrosinase. *J Biol Chem*. 1997;272(42):26226–26235.
22. Isenberg SJ. Macular development in the premature infant. *Am J Ophthalmol*. 1986;101(1):74–80.
23. Abramov I, Gordon J, Hendrickson A, Hainline L, Dobson V, LaBossiere E. The retina of the newborn human infant. *Science*. 1982;217(4556):265–267.
24. Yuodelis C, Hendrickson A. A qualitative and quantitative analysis of the human fovea during development. *Vision Res*. 1986;26(6):847–855.
25. Rosemblat S, Durham-Pierre D, Gardner JM, Nakatsu Y, Brilliant MH, Orlow SJ. Identification of a melanosomal membrane protein encoded by the pink-eyed dilution (type II oculocutaneous albinism) gene. *Proc Natl Acad Sci U S A*. 1994;91(25):12071–12075.
26. Sidman RL, Pearlstein R, Waymouth C. Pink-eyed dilution (p) gene in rodents: increased pigmentation in tissue culture. *Dev Biol*. 1965;12(1):93–116.
27. Lopez VM, Decatur CL, Stamer WD, Lynch RM, McKay BS. L-DOPA is an endogenous ligand for OA1. *PLoS Biol*. 2008;6(9):e236.
28. Lock EA, et al. From toxicological problem to therapeutic use: the discovery of the mode of action of 2-(2-nitro-4-trifluoromethylbenzoyl)-1,3-cyclohexanedione (NTBC), its toxicology and development as a drug. *J Inherit Metab Dis*. 1998;21(5):498–506.
29. Lock EA, Gaskin P, Ellis M, Provan WM, Smith LL. Tyrosinemia produced by 2-(2-nitro-4-trifluoromethylbenzoyl)-cyclohexane-1,3-dione (NTBC) in experimental animals and its relationship to corneal injury. *Toxicol Appl Pharmacol*. 2006;215(1):9–16.
30. Lock EA, Gaskin P, Ellis MK, McLean Provan W, Robinson M, Smith LL. Tissue distribution of 2-(2-nitro-4-trifluoromethylbenzoyl)-cyclohexane-1,3-dione (NTBC) and its effect on enzymes involved in tyrosine catabolism in the mouse. *Toxicology*. 2000;144(1–3):179–187.
31. Lock EA, et al. Tissue distribution of 2-(2-nitro-4-trifluoromethylbenzoyl)cyclohexane-1-3-dione (NTBC): effect on enzymes involved in tyrosine catabolism and relevance to ocular toxicity in the rat. *Toxicol Appl Pharmacol*. 1996;141(2):439–447.
32. Lock EA, Gaskin P, Ellis MK, Robinson M, Provan WM, Smith LL. The effect of a low-protein diet and dietary supplementation of threonine on tyrosine and 2-(2-nitro-4-trifluoromethylbenzoyl) cyclohexane-1,3-dione-induced corneal lesions, the extent of tyrosinemia, and the activity of enzymes involved in tyrosine catabolism in the rat. *Toxicol Appl Pharmacol*. 1998;150(1):125–132.
33. Introne WJ, et al. A 3-year randomized therapeutic trial of nitisinone in alkaptonuria. *Mol Genet Metab*. 2011;103(4):307–314.
34. Suwannarat P, et al. Use of nitisinone in patients with alkaptonuria. *Metabolism*. 2005;54(6):719–728.
35. Green EL. Albino-2J (c<2J>). *Mouse News Lett*. 1973; 49:31.
36. le Fur N, Kelsall SR, Mintz B. Base substitution at different alternative splice donor sites of the tyrosinase gene in murine albinism. *Genomics*. 1996; 37(2):245–248.
37. Kidson SH, Fabian BC. The effect of temperature on tyrosinase activity in Himalayan mouse skin. *J Exp Zool*. 1981;215(1):91–97.
38. Kwon BS, Halaban R, Chintamaneni C. Molecular basis of mouse Himalayan mutation. *Biochem Biophys Res Commun*. 1989;161(1):252–260.
39. Kidson S, Fabian B. Pigment synthesis in the Himalayan mouse. *J Exp Zool*. 1979;210(1):145–152.
40. Garcia-Borron JC, Solano F. Molecular anatomy of tyrosinase and its related proteins: beyond the histidine-bound metal catalytic center. *Pigment Cell Res*. 2002;15(3):162–173.
41. Gaykema WP, Volbeda A, Hol WG. Structure determination of Panulirus interruptus haemocyanin at 3.2 A resolution. Successful phase extension by sixfold density averaging. *J Mol Biol*. 1986;187(2):255–275.
42. Klabunde T, Eicken C, Sacchettini JC, Krebs B. Crystal structure of a plant catechol oxidase containing a dicopper center. *Nat Struct Biol*. 1998; 5(12):1084–1090.
43. Schweikardt T, Olivares C, Solano F, Jaenicke E, Garcia-Borron JC, Decker H. A three-dimensional

model of mammalian tyrosinase active site accounting for loss of function mutations. *Pigment Cell Res.* 2007;20(5):394–401.
44. Sendovski M, Kanteev M, Ben-Yosef VS, Adir N, Fishman A. First structures of an active bacterial tyrosinase reveal copper plasticity. *J Mol Biol.* 2011; 405(1):227–237.
45. Matoba Y, Kumagai T, Yamamoto A, Yoshitsu H, Sugiyama M. Crystallographic evidence that the dinuclear copper center of tyrosinase is flexible during catalysis. *J Biol Chem.* 2006;281(13):8981–8990.
46. Henikoff S, Henikoff JG. Amino acid substitution matrices from protein blocks. *Proc Natl Acad Sci U S A.* 1992;89(22):10915–10919.
47. Grantham R. Amino acid difference formula to help explain protein evolution. *Science.* 1974; 185(4154):862–864.
48. Bennett DC, Cooper PJ, Dexter TJ, Devlin LM, Heasman J, Nester B. Cloned mouse melanocyte lines carrying the germline mutations albino and brown: complementation in culture. *Development.* 1989; 105(2):379–385.
49. King RA, et al. Tyrosinase gene mutations in oculocutaneous albinism 1 (OCA1): definition of the phenotype. *Hum Genet.* 2003;113(6):502–513.
50. Jimenez M, Maloy WL, Hearing VJ. Specific identification of an authentic clone for mammalian tyrosinase. *J Biol Chem.* 1989;264(6):3397–3403.
51. Jimenez-Cervantes C, Garcia-Borron JC, Valverde P, Solano F, Lozano JA. Tyrosinase isoenzymes in mammalian melanocytes. 1. Biochemical characterization of two melanosomal tyrosinases from B16 mouse melanoma. *Eur J Biochem.* 1993;217(2):549–556.
52. Kong KH, Park SY, Hong MP, Cho SH. Expression and characterization of human tyrosinase from a bacterial expression system. *Comp Biochem Physiol B Biochem Mol Biol.* 2000;125(4):563–569.
53. Han HY, Lee JR, Xu WA, Hahn MJ, Yang JM, Park YD. Effect of Cl- on tyrosinase: complex inhibition kinetics and biochemical implication. *J Biomol Struct Dyn.* 2007;25(2):165–171.
54. Hill HZ, Li W, Xin P, Mitchell DL. Melanin: a two edged sword? *Pigment Cell Res.* 1997;10(3):158–161.
55. Guillery RW, Mason CA, Taylor JS. Developmental determinants at the mammalian optic chiasm. *J Neurosci.* 1995;15(7 pt 1):4727–4737.
56. Rachel RA, Mason CA, Beermann F. Influence of tyrosinase levels on pigment accumulation in the retinal pigment epithelium and on the uncrossed retinal projection. *Pigment Cell Res.* 2002;15(4):273–281.
57. Hendrickson A, Provis J. Comparison of development of the primate *fovea centralis* with peripheral retina. In: Sernagor E, Eglen S, Harris B, Wong R, eds. *Retinal Development.* Cambridge, United Kingdom: Cambridge University Press; 2006:126–149.
58. Prusky GT, Alam NM, Beekman S, Douglas RM. Rapid quantification of adult and developing mouse spatial vision using a virtual optomotor system. *Invest Ophthalmol Vis Sci.* 2004;45(12):4611–4616.
59. Russell-Eggitt I, Kriss A, Taylor DS. Albinism in childhood: a flash VEP and ERG study. *Br J Ophthalmol.* 1990;74(3):136–140.
60. Tanguay RM, Lambert M, Grompe M, Mitchell G. Hypertyrosinemia. In: Scriver CR, Beaudet AL, Sly WS, Valle D, eds. *The Metabolic and Molecular Basis of Inherited Disease.* New York, New York, USA: McGraw–Hill; 2001:1777–1805.
61. Abola E, Bernstein FC, Bryant SH, Koetzle TF, Weng J. Protein data bank. In: Bergerhoff G, Sievers, eds. *Crystallographic databases–information content, software systems, scientific applications.* Cambridge, United Kingdom: Data Comission on the International Union of Crystallography; 1987:107–132.
62. Pettersen EF, et al. UCSF Chimera--a visualization system for exploratory research and analysis. *J Comput Chem.* 2004;25(13):1605–1612.
63. Needleman SB, Wunsch CD. A general method applicable to the search for similarities in the amino acid sequence of two proteins. *J Mol Biol.* 1970; 48(3):443–453.
64. Lee C, Subbiah S. Prediction of protein side-chain conformation by packing optimization. *J Mol Biol.* 1991; 217(2):373–388.
65. Lee C. Predicting protein mutant energetics by self-consistent ensemble optimization. *J Mol Biol.* 1994;236(3):918–939.
66. Schultz J, Milpetz F, Bork P, Ponting CP. SMART, a simple modular architecture research tool: identification of signaling domains. *Proc Natl Acad Sci U S A.* 1998;95(11):5857–5864.
67. Letunic I, Doerks T, Bork P. SMART 6: recent updates and new developments. *Nucleic Acids Res.* 2009; 37(Database issue):D229–D232.
68. Levitt M. Accurate modeling of protein conformation by automatic segment matching. *J Mol Biol.* 1992; 226(2):507–533.
69. Laskowski RA, MacArthur MW, Moss DS, Thornton JM. PROCHECK: a program to check the stereochemical quality of protein structures. *J Appl Crystallogr.* 1993;26:283–291.
70. Olivares C, Jimenez-Cervantes C, Lozano JA, Solano F, Garcia-Borron JC. The 5,6-dihydroxyindole-2-carboxylic acid (DHICA) oxidase activity of human tyrosinase. *Biochem J.* 2001;354(pt 1):131–139.
71. Slominski A, Paus R, Costantino R. Differential expression and activity of melanogenesis-related proteins during induced hair growth in mice. *J Invest Dermatol.* 1991;96(2):172–179.
72. King RA. Oculocutaneous albinism type 1. In: Pagon R, ed. *GeneReviews.* Seattle, Washington, USA: University of Washington; 1993.